Dalton Transactions

PAPER

View Article Online
View Journal | View Issue

Cite this: *Dalton Trans.*, 2019, **48**, 16562

Coexistence of Cu(II) and Cu(I) in Cu ion-doped zeolitic imidazolate frameworks (ZIF-8) for the dehydrogenative coupling of silanes with alcohols†

Yan Dai, *[a,b] Peng Xing,‡[a,c] Xiaoqin Cui,[a,c] Zhihong Li[a,c] and Xianming Zhang *[a,d]

Received 5th August 2019,
Accepted 7th October 2019

DOI: 10.1039/c9dt03181b

rsc.li/dalton

Recently, metal-ion-doped zeolitic imidazolate frameworks have gained considerable attention for their structure tailorability and potential catalytic applications. Herein, Cu ion-doped ZIF-8 nanocrystals were successfully prepared by the mechanical grinding of $Cu(NO_3)_2$, ZnO and 2-methylimidazole (HMeIM) using ethanol as an additive. In contrast to the general view that only Cu(II) is present in Cu-doped ZIF-8, we found the coexistence of Cu(II) and Cu(I) in this material, which was supported by XPS and X-ray induced Auger electron spectroscopy (XAES) characterizations. Moreover, ethanol might have acted as a reducer to induce the reduction of Cu(II) during synthesis. Due to the mixed valency of Cu ions, the Cu ion-doped ZIF-8 nanocrystals showed excellent catalytic performance in the dehydrogenative coupling of silanes with alcohols.

1. Introduction

With the ongoing in-depth research on metal organic frameworks (MOFs), many scientists are increasingly focusing on stable MOFs.[1–5] On account of the permanent pores, high surface area and excellent stability of ZIF-8, much effort has been devoted to its synthesis and property research.[6–8] Recently, ZIF-8 has been widely used in designing multifunctional catalysts by forming complexes with noble metals.[9–11] Further, researchers found that doping other metal ions into ZIF-8 is an effective method for the synthesis of functional materials.[12–18] Cu(II) and Co(II) are usually selected for doping in ZIF-8 as their ionic radii are similar to that of Zn(II). Moreover, Cu and Co are common metal active sites in many catalytic reactions, such as hydrogenation reactions, electrocatalytic reactions and coupling reactions.

Dehydrogenative coupling of silanes with alcohols is widely used for preparing silylating agents and surface modification reagents. Previously, noble metals, such as palladium,[19] silver,[20] and gold,[21–24] were generally used as catalysts for this reaction. Recently, the abundant first-row transition metals, such as Co[25] and Cu,[26–29] have been chosen as alternatives to noble metals. Interestingly, researches have implied that both Cu(I) and Cu(II) are active sites for this reaction.[26,29]

In this study, Cu ion-doped ZIF-8 nanocrystals were successfully synthesized by a facile liquid-assisted grinding approach. The EPR results corroborated the presence of Cu(II) in the Cu ion-doped ZIF-8 nanocrystals, whereas XPS and XAES characterizations demonstrated that Cu(I) also existed in this material, evidently different from former studies, which only reported the presence of Cu(II) in Cu ion-doped ZIF-8 crystals. The presence of mixed-valence Cu(I)/Cu(II) in the Cu ion-doped ZIF-8 nanocrystals made us further explore the catalytic properties in the dehydrogenative coupling of silanes. Just as expected, immobilizing both Cu(II) and Cu(I) in the ZIF-8 nanocrystals proved to be an effective strategy in fabricating an excellent Cu-based catalyst for the dehydrogenative coupling reaction. For example, Cu85%ZIF-8 nanocrystals gave a TOF of 34.9 h^{-1} for the dehydrogenative coupling of dimethylphenylsilane with *n*-butanol, and still exhibited high stability after 5 cycles of reaction.

2. Experimental section

2.1. Materials

The chemical reagents used in the experiments were as follows: copper nitrate trihydrate ($Cu(NO_3)_2{\cdot}3H_2O$, 99.9%,

[a]*Institute of Crystalline Materials, Shanxi University, 030006 Taiyuan, China. E-mail: xmzhang@sxu.edu.cn, ydai@sxu.edu.cn*
[b]*State Key Laboratory of Physical Chemistry of Solid Surfaces, Xiamen University, 361005 Xiamen, China*
[c]*Institute of Molecular Science, Shanxi University, 030006 Taiyuan, China*
[d]*School of Chemistry and Material Science, Shanxi Normal University, 041004 Linfen, China*

†Electronic supplementary information (ESI) available. See DOI: 10.1039/c9dt03181b

‡Co-first author.

Sinopharm Chemical Reagent Co., Ltd), zinc oxide (ZnO, Alfa Aesar), 2-methylimidazole (HMeIm, 99%, Ourchem), Ethanol (CH_3CH_2OH, 99.7%, CHEMICAL REAGENT), cupric oxide (CuO, 98%, Innochem), cuprous oxide (Cu_2O, Sinopharm Chemical Reagent Co., Ltd), zinc nitrate hexahydrate ($Zn(NO_3)_2{\cdot}6H_2O$, 99%, Sinopharm Chemical Reagent Co., Ltd), dimethylphenylsilane ($PhMe_2SiH$, 97%, Energy Chemical), *n*-butanol (n-C_4H_9OH, 99.5%, CHEMICAL REAGENT), anisole (C_7H_8O, 99%, Energy Chemical), phenylsilane ($PhSiH_3$, 97%, Energy Chemical), diphenylsilane (Ph_2SiH_2, 98%, Energy Chemical), triphenylsilane (Ph_3SiH, 97%, Energy Chemical), methanol (CH_3OH, 99.5%, CHEMICAL REAGENT), *n*-hexanol (n-$C_6H_{13}OH$, 98%, TCI), and isophthalic acid (HBTC, 99%, Jinan Henghua Technology Co., Ltd). All the reagents and materials were used as received without further purification.

2.2. Preparation

Synthesis of Cu ion-doped ZIF-8 nanocrystals. The reactions were performed by placing a 1 : 4 mixture of metal precursors (ZnO and $Cu(NO_3)_2$) and ligand (HMeIm) in a 50 mL Teflon tank together with liquid ethanol (1 mL), and four 5 mm and four 8 mm stainless steel balls. The mixture was ground for 45 min in a DECO-PBM-V-0.4 L mill at 20 Hz. Then, the products were washed with ethanol three times and separated by centrifugation (12 000 rpm, 1 min). The solid was dried overnight at 80 °C. The finally obtained solid was stored in a glass bottle at room temperature for further use.

Synthesis of ZIF-8 nanocrystals. The reaction was performed at the same conditions used for Cu ion-doped ZIF-8 nanocrystals but without the addition of $Cu(NO_3)_2$.

Synthesis of HKUST-1. HKUST-1 was prepared by using the method reported by Huo with modifications.[30] Isophthalic acid (HBTC, 2 mol) was dispersed in water (10 mL). Then, $Cu(NO_3)_2{\cdot}3H_2O$ (1 mol) was added, and the mixture was stirred at room temperature for 1 h. After the reaction, the final solution was centrifuged. The product obtained after centrifugation was washed using ethanol (3 × 30 mL) and then, dried at 80 °C for 12 h.

Synthesis of $Cu(Im)_2$. Cu $(Im)_2$ was synthesised according to the report of N. Masciocchi *et al.*[31] First, 2.50 mmol $Cu(NO_3)_2{\cdot}3H_2O$ and 29.4 mmol of imidazole were dissolved in 50 mL water. Then, NaOH (0.1 M) was added to the above solution until a reddish-purple precipitate was observed. After filtering, the powder was washed with ethanol and dried under vacuum at 80 °C. Finally, the powder was heated at 215 °C for 8 h under a nitrogen atmosphere.

Synthesis of $Cu(2\text{-}MeIm)_2$. 1.6 mmol of $Cu(NO_3)_2{\cdot}3H_2O$ and 6.4 mmol of 2-methylimidazole were placed in a grinding vessel, followed by the addition of 1 mL of ethanol. Then, the mixture was milled for 45 min. After grinding, the product was transferred to a centrifuge tube and washed using an ethanol and *n*-hexane mixture (1 : 8) for three times. The product was dried overnight at 80 °C.

Synthesis of zero-valence Cu. Zero-valence Cu was synthesized by reducing Cu85%ZIF-8 with hydrazine. In detail, 50 mg Cu85%ZIF-8 was placed in a glass bottle, followed by the addition of 2 mL of *n*-butanol. Then, 100 μL hydrazine was added to the above solution, and the mixture was stirred at 70 °C for 2 h. After the reaction, the products were washed using *n*-butanol three times and separated by centrifugation.

2.3. Characterization

Powder X-Ray Diffraction (PXRD) measurements were recorded on a Rigaku Ultima IV diffractometer using Cu Kα radiation and a graphite monochromator (λ = 1.54056 Å) at 40 kV voltage and 40 mA current at the scan speed of 10° min^{-1} with a step size of 0.02°. The morphology of the samples was observed using a JEOL-JSM-6701 field-emission scanning microscope (SEM), operating at an accelerating voltage of 10 kV and an FEI Tecnai G2 F20S-Twin transmission electron microscope (TEM) at an accelerating voltage of 200 kV. The Cu molar percentage in Cu/ZIF-8 was determined by a NexION 350 inductively coupled plasma mass spectrometer (ICP-MS). X-ray photoelectron spectroscopy (XPS) and X-ray excited Auger electron spectroscopy (XAES) were performed on a PHI-5702 instrument, and the C_{1s} line at 284.6 eV was used as the binding energy reference. The electron paramagnetic resonance (EPR) spectra were recorded at 293 K with the following parameters: frequency: 9.86 GHz, power: 5.02 mW, modulation amplitude: 4 G, modulation frequency: 100 kHz, center field, 3320.00 G. The N_2 adsorption–desorption isotherms were recorded on a Quantachrome autosorb iQ instrument; a liquid nitrogen bath (77 K) and ultra-high purity grade nitrogen were used through the nitrogen adsorption experiments. All the samples were degassed under vacuum at 423 K for 6 h before the test. In order to calculate the apparent surface areas, the multipoint Braunauer–Emmett–Teller (BET) method was applied using the adsorption branches of the N_2 isotherms, and the pore size distribution was analyzed by the Barrett Joyner Halenda (BJH) method. The pore volume was calculated by the total pore volume (TPV) method. FT-IR spectra were recorded using a Nicolet iS5 FTIR system, and potassium bromide was used to form sample mirrors. Thermogravimetric analysis (TGA) was performed on a Setaram Labsys Evo apparatus. The samples were heated in an alumina pan from 30 °C to 800 °C at a heating rate of 10 °C min^{-1} under an N_2 atmosphere.

2.4. Catalytic performance tests

The Cu ion-doped ZIF-8 nanocrystals (50 mg) were charged in a 25 mL reinforced glass reactor equipped with a magnetic bar. Then, alcohol was added (2 mL). Finally, the silane (1 mmol) was introduced in the reactor using a syringe. The reaction mixture was stirred at 70 °C for the required time was and cooled down to room temperature, and the catalyst was removed by centrifugation. For GC analysis, a known amount of anisole (0.5 mmol) was added as the internal standard. A gas chromatography system (FULI 9790II) was equipped with a KB-5 capillary column and an FID detector to monitor the progress of the silane dehydrogenation coupling reaction.

3. Results and discussion

3.1. Synthesis and characterization of Cu ion-doped ZIF-8 nanocrystals

In this study, we synthesized Cu ion-doped ZIF-8 nanocrystals *via* a facile liquid-assisted grinding approach.[32,33] In detail, the synthesis was performed in a grinding machine by mixing ZnO, $Cu(NO_3)_2$ and four-fold HMelm with a small amount of alcohol at room temperature for 45 min. Molar percentages of 25%, 55% and 85% Cu to all metal elements were used in these experiments, and the products were denoted as Cu25% ZIF-8, Cu55%ZIF-8, and Cu85%ZIF-8, respectively. As displayed in Fig. 1a, the Cu ion-doped ZIF-8 nanocrystals had identical XRD patterns with ZIF-8, which indicated that the parent framework of ZIF-8 was maintained after doping with Cu ions. Further, the permanent porosity of the Cu ion-doped ZIF-8 nanocrystals was demonstrated by N_2 adsorption at 77 K (Fig. S1 and Table S1†). For all three Cu ion-doped ZIF-8 samples, type I isotherms were obtained, indicating a microporous structure. The actual Cu content in Cu25%ZIF-8, Cu55%ZIF-8 and Cu85%ZIF-8 determined by ICP-MS were 6.4%, 9.1% and 16.8%, respectively (molar percentages of Cu to all metal elements). From the photographs of the powder samples (the inset of Fig. 1a), we found that as the doping percentage of Cu increased from 25% to 85%, the sample color changed from light yellow-green to dark yellow-green.

In subsequent analysis, the presence of Cu ions in the sample was further confirmed by UV-visible spectroscopy. As shown in Fig. 1b, doping caused the absorption edge of Cu-doped ZIF-8 to move from the UV to the visible region. Moreover, the first definite band of the Cu ion-doped ZIF-8 nanocrystals was located at around 460.0 nm, while the second broad band started at 600 nm and extended to the infrared region. Moreover, the first absorption band was blue-shifted from 467.0 nm to 454.5 nm as the doping percentage of Cu ions increased from 25% to 85%. Further, TEM was conducted to characterize the size distribution of the Cu ion-doped ZIF-8 nanocrystals. The TEM images in Fig. S2† revealed that the mechanochemical method used in this study did not have much advantage in controlling the size of nanocrystals. However, this synthesis method greatly reduced the amount of solvent used and can be easily implemented for large-scale synthesis. Furthermore, the thermal stability of Cu ion-doped ZIF-8 under the N_2 atmosphere reduced after Cu doping. For example, the thermal decomposition temperature of Cu85%ZIF-8 reduced from 430 °C to 320 °C compared with ZIF-8 (Fig. S3†).

From the above results, it was confirmed that the Cu ions were indeed doped into the ZIF-8 nanocrystals. However, the valence state of the Cu ions was still unknown. Therefore, EPR, XPS and XAES characterization were further performed. First, the EPR spectrum of Cu85%ZIF-8 (Fig. 2a) exhibited a pronounced peak at $g_{\perp} = 2.095$ and a poorly resolved double peak at $g_{\parallel} = 2.321$, corresponding to isolated Cu(II). The EPR spectra of Cu55%ZIF-8 and Cu25%ZIF-8 were similar to that of Cu85% ZIF-8, and the corresponding anisotropic parameters are summarized in Table S2.†

Then, XPS spectroscopy was performed to characterize the oxidation state of Cu ions in the surface region. As displayed in Fig. 2b, the coexistence of Cu(I) and Cu(II) in Cu85%ZIF-8 was evidenced by a shoulder observed on the main peak at 932.5 eV, which could be assigned to the Cu(I) species.[34] The higher binding energy (BE) Cu $2p_{3/2}$ peak at 934.6 eV was due to Cu(II),[35] and the Cu $2p_{1/2}$ peaks at 952.4 eV and 954.6 eV were assigned to Cu(I) and Cu(II), respectively. Further, as shown in Fig. S4,† the XPS spectra of Cu25%ZIF-8 and Cu55% ZIF-8 were similar to that of Cu85%ZIF-8. These results implied that Cu(I) and Cu(II) coexisted in the Cu ion-doped ZIF-8 nanocrystals.

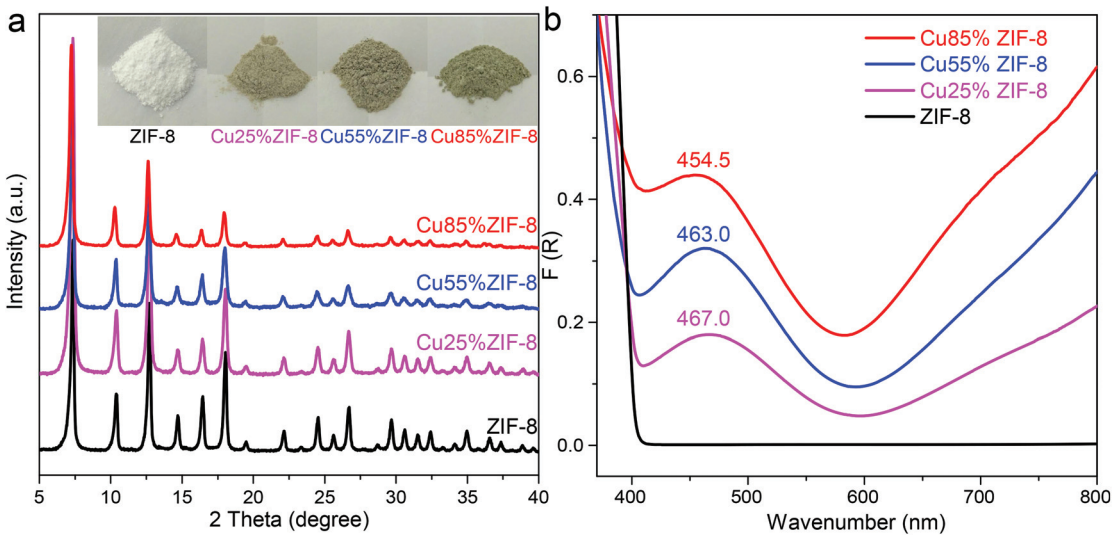

Fig. 1 (a) XRD patterns of Cu ion-doped ZIF-8 nanocrystals prepared with different contents of Cu. Data for ZIF-8 is also given for comparison. The inset of a shows the photographs of the corresponding samples. (b) Diffuse reflectance absorption spectra of ZIF-8 and the Cu ion-doped ZIF-8 nanocrystals.

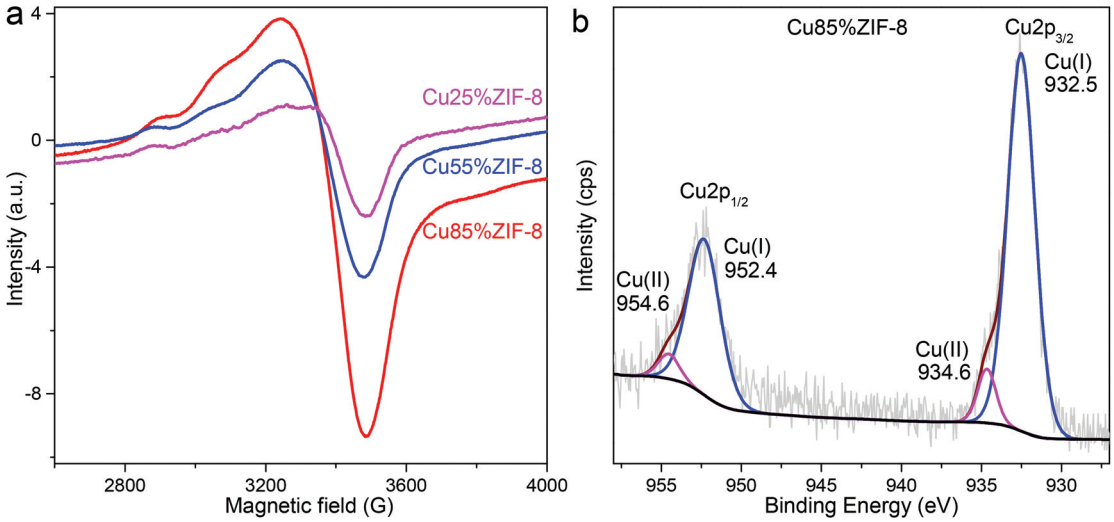

Fig. 2 (a) EPR spectra of the Cu ion-doped ZIF-8 nanocrystals; (b) Cu 2p XPS spectrum of the Cu85%ZIF-8 nanocrystals (gray line: raw data; wine line: fitted peak plot; blue line: fitted Cu(I) peak plot; magenta line: fitted Cu(II) peak plot and black line: background).

To further confirm the presence of Cu(I) in the Cu ion-doped ZIF-8 nanocrystals, the XAES spectra of these samples were also analyzed. As shown in Fig. S5,† in the Cu85%ZIF-8 spectrum, the peak at E_k = 915.3 eV (kinetic energy) was attributed as the characteristic peak of Cu(I).[34] In the Cu55%ZIF-8 and Cu25%ZIF-8 spectra, it was hard to figure out the peak of Cu(I) from the raw data, perhaps because of the low content of Cu(I) in these samples.

Therefore, from the EPR, XPS and XAES characterization results, we confirmed that Cu(I) and Cu(II) coexisted in the Cu ion-doped ZIF-8 nanocrystals. During the synthesis process, both Cu(II) and Zn(II) could coordinate with four 2-methylimidazolium *via* a coordination bond between the metal and nitrogen atoms. Thus, the question of why Cu(I) is present in Cu ion-doped ZIF-8 arises. According to previous reports on Cu-based coordination polymers,[36,37] we speculated that the small amount of liquid (ethanol) used in the synthesis may act as the reducing agent to induce the reduction of Cu(II) to Cu(I). Although the synthesis was performed at room temperature, local short-range heating could have been induced by mechanochemistry, which is advantageous for the reduction of Cu(II). Furthermore, IR characterization was conducted to prove that Cu is coordinated with the ligand (HMeIm). As shown in Fig. S6,† the IR band, corresponding to the metal–nitrogen stretching frequency in Cu85%ZIF-8 (ν_{Cu-N}), was blue-shifted compared to that in ZIF-8 (ν_{Zn-N}), which implied that the Cu–N bonds were more rigid than the Zn–N bonds. Since the electronegativity of copper is higher than that of zinc (1.90 *vs.* 1.65), the Cu–N bonds are more ionic than the Zn–N bonds and therefore are stiffer, resulting in the blue-shift of ν_{M-N} in the IR spectra.[38]

3.2. Catalytic dehydrogenative coupling of silanes with alcohols

After successfully confining Cu(I) and Cu(II) in ZIF-8 *via* the liquid-assisted grinding approach, we tried to study the catalytic properties of the material. Since both Cu(I) and Cu(II) are active sites for the dehydrogenative coupling of silanes with alcohols,[29] the catalytic performance of Cu(I)/Cu(II) co-doped ZIF-8 nanocrystals in this reaction was first evaluated. Initially, $PhMe_2SiH$ and *n*-butanol were selected as the model substrates for the reaction, and the results are presented in Table 1.

First, we found that the Cu ion-doped ZIF-8 nanocrystals with different Cu doping percentages had nearly identical TOFs (about 35.0 h^{-1}, entries 1 to 3). These results indicated that the three studied Cu ion-doped ZIF-8 nanocrystals had the same active sites. As Cu85%ZIF-8 had the highest Cu content and exhibited a short reaction time of 14 h, attention was paid to this material in the following experiments.

Initially, the influence of catalyst mass and reaction temperature on the catalytic performance of Cu85%ZIF-8 was evalu-

Table 1 Optimization of reaction conditions for the dehydrogenative coupling of $PhMe_2SiH$ and *n*-butanol catalyzed by Cu ion-doped ZIF-8 nanocrystals[a]

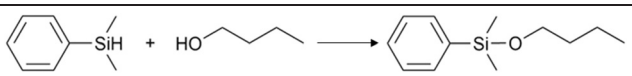

Entry	Catalyst	Time/h	Conv.[b]/%	Sel.[b]/%	TOF[b]/h^{-1}
1	Cu25%ZIF-8[c]	75	100	100	35.0
2	Cu55%ZIF-8[c]	26	100	100	34.6
3	Cu85%ZIF-8[c]	14	100	100	34.9
4	Cu85%ZIF-8[d]	65	100	100	35.4
5	Cu85%ZIF-8[e]	122	68	100	26.0
6	Cu85%ZIF-8[f]	9	100	100	43.6

[a] Reaction conditions: $PhMe_2SiH$ (1.0 mmol), 2 mL of *n*-butanol. [b] Conversion of $PhMe_2SiH$ was determined by GC analysis using anisole as the internal standard, and the product was siloxane. TOF was calculated based on the conversion of $PhMe_2SiH$ at 30%, TOF = moles of converted $PhMe_2SiH$/(moles of Cu × time). [c] 50 mg Cu ion-doped ZIF-8 nanocrystals, 70 °C. [d] 25 mg Cu85%ZIF-8 (20 μmol Cu), 70 °C. [e] 50 mg Cu85%ZIF-8, 30 °C. [f] 50 mg Cu85%ZIF-8, 110 °C.

ated. When the mass of Cu85%ZIF-8 was reduced from 50 mg to 25 mg, although the TOF of Cu85%ZIF-8 remained almost unchanged (35.4 h^{-1}), the time for the total conversion of $PhMe_2SiH$ prolonged from 14 h to 65 h (entry 4). Moreover, when the reaction temperature was lowered from 70 °C to 30 °C, the TOF of Cu85%ZIF-8 decreased to 26 h^{-1} (entry 5). Raising the reaction temperature to 110 °C resulted in a higher TOF of 43.6 h^{-1} (entry 6). In this case, however, the supernatant liquid appeared blue after the reaction, while the normal color of the supernatant was colorless. The blue color could be the color of the Cu ions, which indicates the low stability of the Cu85%ZIF-8 nanocrystals at this critical condition. When Cu85%ZIF-8 was used for the second cycle, the conversion of $PhMe_2SiH$ was only 45%. This result confirmed our speculation that the Cu ions in Cu85%ZIF were lost at 110 °C.

After tuning the reaction parameters to optimize the catalytic performance of Cu85%ZIF-8, the reaction conditions of entry 3 (50 mg catalyst and 70 °C) were chosen for the stability test. It is worth noting that the Cu85% ZIF-8 nanocrystals not only exhibited excellent catalytic performance but also high stability in the reaction. As illustrated in Fig. S7,† the Cu85% ZIF-8 nanocrystals were able to maintain high $PhMe_2SiH$ conversion and siloxane selectivity after 5 cycles. Further, the XPS spectrum of Cu85%ZIF-8 after 5 cycles of reaction indicated that Cu(I) was still present in this material (Fig. S8†).

Moreover, control experiments were conducted to further confirm the role of Cu ion-doped ZIF-8 in the catalytic reaction. The blank experiment (without catalyst) could convert only 1.0% of $PhMe_2SiH$ (Table S3,† entry 1), and the ZIF-8 nanocrystals converted 4.4% of $PhMe_2SiH$ (Table S3,† entry 2). Both these results are poorer than that of Cu85%ZIF-8, which resulted in the complete conversion of $PhMe_2SiH$ at the same conditions. These results indicated that the catalytic activity of Cu ion-doped ZIF-8 was mainly derived from the Cu species.

From the above discussion, it is clear that the Cu ion-doped ZIF-8 nanocrystals had high catalytic activity and stability in the dehydrogenative coupling of dimethylphenylsilane with *n*-butanol. For comparison, we further tested the catalytic performance of other Cu-based materials. As indicated in Table 2, Cu-based materials with a Cu–O bond had low TOFs in this reaction (entries 1 to 3). In detail, commercial CuO and Cu_2O were used as received, and the average particle sizes of CuO (entry 1) and Cu_2O (entry 2) were 52 nm and 47 nm, respectively. For entry 3, the HKUST-1 ($[Cu_3(BTC)_2]$), a Cu-based MOF, was synthesized according to the modified version of the method reported by Huo (XRD pattern of HKUST-1 in Fig. S9†).[30] The Cu 2p XPS spectrum of HKUST-1 revealed the coexistence of Cu(II) and Cu(I) in this material (Fig. S10†). Compared with Cu85%ZIF-8 nanocrystals, HKUST-1 had a lower TOF (3.5 h^{-1}) under the same conditions (entry 3). A previous study by A. Dhakshinamoorthy *et al.* had revealed that HKUST-1 exhibited excellent catalytic activity for this reaction, and both Cu(II) and Cu(I) were simultaneously required as active sites.[29] We also evaluated the catalytic activity of HKUST-1 under the same conditions as the report (entry 4) and got the same results. We speculated that the lower TOF of HKUST-1 in entry 3 could be mainly because of the lower catalyst mass used here. The above results indicated that the three Cu-based materials with Cu–O bonds exhibited poor catalytic activity than the Cu-doped ZIF-8 nanocrystals under the same reaction conditions, regardless of the valence state of the Cu ions.

Table 2 Catalytic properties of other Cu-based materials[a]

Entry	Catalyst	Time/h	Conv./%	Sel.[b]/%	TOF/h^{-1}
1	CuO	97	80	100	8.2
2	Cu_2O	54	100	100	5.1
3	HKUST-1	48	100	97	3.5
4	HKUST-1[c]	0.25	100	100	20
5	$Cu(Im)_2$	118	100	100	2.9
6	$Cu(2\text{-}MeIm)_2$	17	100	98	7.1
7	$Cu(NO_3)_2{\cdot}3H_2O$	5	95	86	44.4
8	$Cu(NO_3)_2{\cdot}3H_2O$	15	100	85	44.4
9	Cu	68	99	99	0.7

[a] Reaction conditions: $PhMe_2SiH$ (1.0 mmol), 2 mL of *n*-butanol, 40 μmol Cu, at 70 °C. [b] The by-product was dimethyl phenyl silanol. [c] Reaction conditions: $PhMe_2SiH$ (1.0 mmol), 2 mL of *n*-butanol, 267 μmol Cu, 70 °C.

Further, the Cu-based coordination polymers $Cu(Im)_2$ and $Cu(2\text{-}MeIm)_2$ (Im = imidazole, 2-MeIm = 2-methylimidazole) with Cu–N bonds were also evaluated for the influence of the chemical environment of Cu ions on their catalytic performance. $Cu(Im)_2$ was synthesized according to the report of N. Masciocchi.[31] The method for the synthesis of $Cu(2\text{-}MeIm)_2$ was the same as that for the Cu ion-doped ZIF-8 nanocrystals but without the addition of Zn $(NO_3)_2$. Only Cu(II) existed in $Cu(Im)_2$[31] and $Cu(2\text{-}MeIm)_2$ (XPS spectrum in Fig. S11†), and the Cu(II) in $Cu(Im)_2$ coordinated with four HIm molecules *via* Cu–N bonds. For $Cu(2\text{-}MeIm)_2$, although the detailed structure is still unknown, its sharp and strong XRD diffraction peak indicated high crystallinity (Fig. S12†). Therefore, we believe that the Cu–N bond is present in $Cu(2\text{-}MeIm)_2$. From entry 5 in Table 2, we knew that $Cu(Im)_2$ exhibited low activity in this reaction (TOF of 2.9 h^{-1}). Compared with $Cu(Im)_2$, $Cu(2\text{-}MeIm)_2$ had a higher TOF of 7.1 h^{-1} (entry 6), which is lower than that of the Cu ion-doped ZIF-8 nanocrystals. We speculated that the presence of only Cu(II) in these two coordination polymers could be a reason for their poor activity compared with the Cu ion-doped ZIF-8 nanocrystals. The synergy between Cu(II) and Cu(I) is important for the catalytic dehydrogenative coupling of silanes with alcohols.

Finally, the catalytic performance of $Cu(NO_3)_2{\cdot}3H_2O$ and zero-valence Cu were also tested (entries 7–9). The TOF of $Cu(NO_3)_2{\cdot}3H_2O$ was 44.4 h^{-1}, while the selectivity for siloxane was only 85%, and the by-product was dimethyl phenyl silanol. It is worth noting that $Cu(NO_3)_2{\cdot}3H_2O$ displayed an obvious color change during the reaction. After the reaction started, $Cu(NO_3)_2{\cdot}3H_2O$ was reduced to a black solid, and the reaction rate was fast till the conversion of $PhMe_2SiH$ reached 95% after 5 h of reaction (entry 6). Then, the solution turned blue-green, and the reaction rate obviously decreased. The

complete conversion of $PhMe_2SiH$ was reached after 15 h of reaction (entry 7). The obvious color change in $Cu(NO_3)_2{\cdot}3H_2O$ during the catalytic reaction suggested that the active species may be the heterogeneous Cu species (black solid) in the early stage of the reaction. Moreover, zero-valence Cu was synthesized by reducing Cu85%ZIF-8 with hydrazine (the details of the synthesis are given in the Experimental section). As seen in Table 2 entry 9, the TOF of Cu was low (0.7 h^{-1}), which indicated that zero-valence Cu was less active in this reaction.

As discussed above, Cu ion-doped ZIF-8 nanocrystals exhibited high activity and selectivity for the dehydrogenative coupling of $PhMe_2SiH$ and *n*-butanol compared with other Cu-based materials. Moreover, the reaction could be performed under an air atmosphere in contrast to the previously reported Cu-based catalysts (Table S4†). Although the TOF value of the Cu ion doped ZIF-8 nanocrystals was not the highest (compared with that of oriented (2.0.0) copper(I) oxide nanoplatelets on few-layered graphene[28]), we believe that the simple preparation method used for this material is beneficial for its further application. In addition, the Cu ion-doped ZIF-8 nanocrystals exhibited higher catalytic performance than the metal-free N and S co-doped carbon catalyst[39] but lower than those of the Co single atom catalyst[25] and noble metal catalysts[19,22,23] (Table S4†).

Further, the surface ratio of Cu(I) to Cu(II) was calculated based on XPS data to find out the influence of the Cu oxidation state on the catalytic performance (Table S5†). In the Cu ion-doped ZIF-8 nanocrystals, the average surface ratio of Cu(I) to Cu(II) was about 9 : 1, while that in HKUST-1 was about 3 : 7. We speculate that the ratio of Cu(I) to Cu(II) may also play an important role in the reaction, and further research is required for proof.

Based on the above findings, we further extended the reaction range for silane dehydrogenation coupling, and the results are presented in Table 3. When dimethylphenylsilane reacted with methanol, ethanol, *n*-butanol, and *n*-octanol, the reaction time increased as the alkyl chain of the alcohol increased in length (entries 1 to 4). In entries 5 to 7, *n*-butanol reacted with phenylsilane, diphenylsilane, and triphenylsilane, respectively. As the molecular steric hindrance of silane increased, the reaction time was greatly extended. All these reactions completely produced single substituted siloxanes.

Table 3 Results of the dehydrogenative coupling of silanes with alcohols catalyzed by Cu85%ZIF-8

Entry	Silane	Alcohol	Time[a]/h
1	$PhMe_2SiH$[b]	Methanol	6
2	$PhMe_2SiH$[b]	Ethanol	12
3	$PhMe_2SiH$[b]	*n*-Butanol	14
4	$PhMe_2SiH$[b]	*n*-Hexyl alcohol	23
5	$PhSiH_3$[c]	*n*-Butanol	12
6	Ph_2SiH_2[d]	*n*-Butanol	16
7	Ph_3SiH[d]	*n*-Butanol	24

[a] The time for the complete conversion of silanes. [b] Reaction conditions: $PhMe_2SiH$ (1.0 mmol), alcohol (2.0 mL), Cu85%ZIF-8 (50 mg), 70 °C. [c] $PhSiH_3$ (5.0 mmol), *n*-butanol (2.0 mL), Cu85%ZIF-8 (25 mg), 30 °C. [d] Silane (0.1 mmol), *n*-butanol (2.0 mL), Cu85%ZIF-8 (50 mg), 70 °C.

4. Conclusions

Cu ion-doped ZIF-8 nanocrystals were synthesized *via* a solvent-assisted mechanochemical method. From the EPR, XPS and XAES analyses, we found that both Cu(I) and Cu(II) were present in this material, and the surface ratio of Cu(I) to Cu(II) was about 9 : 1. The coexistence of Cu(I) and Cu(II) in the Cu ion-doped ZIF-8 nanocrystals makes them excellent catalysts for the dehydrogenative coupling of silanes with alcohols. We speculate that the ratio of Cu(I) to Cu(II) is also important for the excellent catalytic performance, which requires further research to be proven. Since the valence state of Cu ions also plays an important role in many other reactions, further study is currently underway to apply this material to other catalytic reactions.

Conflicts of interest

There are no conflicts to declare.

Acknowledgements

This work was supported by the Natural Science Foundation for Young Scientists of Shanxi Province, China (201601D021031), Natural Science Foundation of China (21601114 & 20871167) and the Fund for Shanxi "1331" Project. We also wish to acknowledge the Open Project (No. 201614) of The State Key Laboratory of Physical Chemistry of Solid Surfaces (Xiamen University).

Notes and references

1 M.-T. Zhao, K. Yuan, Y. Wang, G.-D. Li, J. Guo, L. Gu, W.-P. Hu, H.-J. Zhao and Z.-Y. Tang, *Nature*, 2016, **539**, 76–80.
2 B. Wang, X.-L. Lv, D.-W. Feng, L.-H. Xie, J. Zhang, M. Li, Y.-B. Xie, J.-R. Li and H.-C. Zhou, *J. Am. Chem. Soc.*, 2016, **138**, 6204–6216.
3 J. Liang, R.-P. Chen, X.-Y. Wang, T.-T. Liu, X.-S. Wang, Y.-B. Huang and R. Cao, *Chem. Sci.*, 2017, **8**, 1570–1575.
4 J.-H. Wang, Y. Zhang, M. Li, S. Yan, D. Li and X.-M. Zhang, *Angew. Chem., Int. Ed.*, 2017, **56**, 6478–6482.
5 X.-S. Wang, C.-H. Chen, F. Ichihara, M. Oshikiri, J. Liang, L. Li, Y.-X. Li, H. Song, S.-Y. Wang, T. Zhang, Y.-B. Huang, R. Cao and J.-H. Ye, *Appl. Catal., B*, 2019, **253**, 323–330.
6 K. S. Park, Z. Ni, A. P. Côté, J. Y. Choi, R. Huang, F. J. Uribe-Romo, H. K. Chae, M. O'Keeffe and O. M. Yaghi, *Proc. Natl. Acad. Sci. U. S. A.*, 2006, **103**, 10186–10191.

7 A. Phan, C. J. Doonan, F. J. Uribe-Romo, C. B. Knobler, M. O'Keeffe and O. M. Yaghi, *Acc. Chem. Res.*, 2010, **43**, 58–67.
8 Y.-R. Lee, M.-S. Jang, H.-Y. Cho, H.-J. Kwon, S. Kim and W.-S. Ahn, *Chem. Eng. J.*, 2015, **271**, 276–280.
9 T. Ma, T.-T. Liu, Y.-Y. Yang, Y.-B. Huang and R. Cao, *Chin. J. Inorg. Chem.*, 2014, **30**, 127–133.
10 Q.-H. Yang, Q. Xu, S.-H. Yu and H.-L. Jiang, *Angew. Chem.*, 2016, **128**, 3749–3753.
11 P. Falcaro, R. Ricco, A. Yazdi, I. Imaz, S. Furukawa, D. Maspoch, R. Ameloot, J. D. Evans and C. J. Doonan, *Coord. Chem. Rev.*, 2016, **307**, 237–254.
12 R. Li, X.-Q. Ren, X. Feng, X.-G. Li, C.-W. Hu and B. Wang, *Chem. Commun.*, 2014, **50**, 6894–6897.
13 A. Schejn, A. Aboulaich, L. Balan, V. Falk, J. Lalevée, G. Medjahdi, L. Aranda, K. Mozet and R. Schneider, *Catal. Sci. Technol.*, 2015, **5**, 1829–1839.
14 M. T. Thanh, T. V. Thien, V. T. T. Chau, P. D. Du, N. P. Hung and D. Q. Khieu, *J. Chem.*, 2017, **2017**, 5045973.
15 K. Zhou, B. Mousavi, Z.-X. Luo, S. Phatanasri, S. Chaemchuen and F. Verpoort, *J. Mater. Chem. A*, 2017, **5**, 952–957.
16 J.-Z. Sun, L. Semenchenko, W. T. Lim, M. F. Ballesteros Rivas, V. Varela-Guerrero and H.-K. Jeong, *Microporous Mesoporous Mater.*, 2018, **264**, 35–42.
17 P.-F. Zhang, Y. Xiao, H. Sun, X.-P. Dai, X. Zhang, H.-X. Su, Y.-C. Qin, D.-W. Gao, A.-X. Jin, H. Wang, X.-B. Wang and S.-G. Sun, *Cryst. Growth Des.*, 2018, **18**, 3841–3850.
18 W. Xu, H. Chen, K.-C. Jie, Z.-Z. Yang, T.-T. Li and S. Dai, *Angew. Chem.*, 2019, **131**, 5072–5076.
19 J.-D. Lin, Q.-Y. Bi, L. Tao, T. Jiang, Y.-M. Liu, H.-Y. He, Y. Cao and Y.-D. Wang, *ACS Catal.*, 2017, **7**, 1720–1727.
20 A. Dhakshinamoorthy, I. N. Esteve Adell, A. Primo and H. Garcia, *ACS Sustainable Chem. Eng.*, 2017, **5**, 2400–2406.
21 T. Taguchi, K. Isozaki and K. Miki, *Adv. Mater.*, 2012, **24**, 6462–6467.
22 M. Takato, Y. Yuya, N. Akifumi, M. Tomoo, J. Koichiro and K. Kiyotomi, *Chem. – Eur. J.*, 2013, **19**, 14398–14402.
23 C. Wang, X.-J. Lin, Y.-Z. Ge, Z. H. Shah, R.-W. Lu and S.-F. Zhang, *RSC Adv.*, 2016, **6**, 102102–102108.
24 M. Dhiman, B. Chalke and V. Polshettiwar, *J. Mater. Chem. A*, 2017, **5**, 1935–1940.
25 X. Wang, P. Li, Z.-J. Li, W.-X. Chen, H. Zhou, Y.-F. Zhao, X.-Q. Wang, L.-R. Zheng, J.-C. Dong, Y. Lin, X.-S. Zheng, W.-S. Yan, J. Yang, Z.-K. Yang, Y.-T. Qu, T.-W. Yuan, Y.-E. Wu and Y.-D. Li, *Chem. Commun.*, 2019, **55**, 6563–6566.
26 H. Ito, A. Watanabe and M. Sawamura, *Org. Lett.*, 2005, **7**, 1869–1871.
27 J. F. Blandez, A. Primo, A. M. Asiri, M. Álvaro and H. García, *Angew. Chem., Int. Ed.*, 2014, **53**, 12581–12586.
28 A. Primo, I. Esteve-Adell, J. F. Blandez, A. Dhakshinamoorthy, M. Álvaro, N. Candu, S. M. Coman, V. I. Parvulescu and H. García, *Nat. Commun.*, 2015, **6**, 8561–8571.
29 A. Dhakshinamoorthy, P. Concepcion and H. Garcia, *Chem. Commun.*, 2016, **52**, 2725–2728.
30 J. Huo, M. Brightwell, S. El Hankari, A. Garai and D. Bradshaw, *J. Mater. Chem. A*, 2013, **1**, 15220–15223.
31 N. Masciocchi, S. Bruni, E. Cariati, F. Cariati, S. Galli and A. Sironi, *Inorg. Chem.*, 2001, **40**, 5897–5905.
32 T. Friščić and L. Fábián, *CrystEngComm*, 2009, **11**, 743–745.
33 P. J. Beldon, L. Fábián, R. S. Stein, A. Thirumurugan, A. K. Cheetham and T. Friščić, *Angew. Chem., Int. Ed. Engl.*, 2010, **49**, 9640–9643.
34 H.-R. Yue, Y.-J. Zhao, S. Zhao, B. Wang, X.-B. Ma and J.-L. Gong, *Nat. Commun.*, 2013, **4**, 2339–2345.
35 J. Fan, Y.-H. Dai, Y.-L. Li, N.-F. Zheng, J.-F. Guo, X.-Q. Yan and G.-D. Stucky, *J. Am. Chem. Soc.*, 2009, **131**, 15568–15569.
36 X.-C. Huang, J.-P. Zhang, Y.-Y. Lin, X.-L. Yu and X.-M. Chen, *Chem. Commun.*, 2004, 1100–1101.
37 Y. Q. Tian, H. J. Xu, L. H. Weng, Z. X. Chen, D. Y. Zhao and X. Z. You, *Eur. J. Inorg. Chem.*, 2004, **2004**, 1813–1816.
38 H. T. Kwon, H.-K. Jeong, A. S. Lee, H. S. An and J. S. Lee, *J. Am. Chem. Soc.*, 2015, **137**, 12304–12311.
39 B.-F. Chen, F.-B. Li, Q.-Q. Mei, Y.-D. Yang, H.-Z. Liu, G.-Q. Yuan and B.-X. Han, *Chem. Commun.*, 2017, **53**, 13019–13022.